J Mater Sci: Mater Electron (2009) 20:105–112
DOI 10.1007/s10854-008-9635-z

Temperature-dependent current–voltage and capacitance–voltage characteristics of the Ag/*n*-InP/In Schottky diodes

F. E. Cimilli · H. Efeoğlu · M. Sağlam · A. Türüt

Received: 18 October 2007 / Accepted: 5 February 2008 / Published online: 29 February 2008
© Springer Science+Business Media, LLC 2008

Abstract The current–voltage (*I–V*) and capacitance–voltage (*C–V*) characteristics of Ag/*n*-InP/In Schottky diodes have been studied in a wide temperature range by steps of 10 K. A decrease in the apparent barrier height (BH), Φ_{bo}, an increase in the ideality factor, *n* and a non-linearity in the activation energy plot with a decrease in temperature have been seen. The experimental values of BH and ideality factor for the devices were calculated as 0.61 eV and 1.18 at 320 K, 0.48 eV and 1.52 at 200 K, and 0.20 eV and 3.89 at 70 K, respectively. An abnormal decrease in the experimental BH Φ_b and an increase in the ideality factor *n* with a decrease in temperature have been explained by the barrier inhomogeneities at the metal–semiconductor (MS) interface. From the temperature dependent *I–V* characteristics of the Ag/*n*-InP contact, that is, $\overline{\Phi}_{bo}$ and *A** as 0.79 and 0.55 eV, and 7.96 and 8.18 A/cm^{2}K^2, respectively, have been calculated from a modified $\ln(I_0/T^2) - q^2\sigma_s^2/2k^2T^2$ vs. $1/T$ plot for the two temperature regions. The Richardson constant values are in close agreement with the value of 9.8 A/cm^{2}K^2 known for *n*-type InP. Moreover, the difference between the apparent BHs obtained from the *I–V* and *C–V* characteristics has been attributed to the existence of Schottky BH inhomogeneity.

F. E. Cimilli · M. Sağlam · A. Türüt (✉)
Faculty of Sciences and Arts, Department of Physics, Atatürk University, 25240 Erzurum, Turkey
e-mail: aturut@atauni.edu.tr

H. Efeoğlu
Faculty of Engineering, Department of Electric and Electronics Engineering, Atatürk University, 25240 Erzurum, Turkey

1 Introduction

The wide band-gap III–V compound semiconductors due to the fabrication of various electronic and optoelectronic devices have important applications in the last years. Metal film deposition on InP substrates semiconductor has received much attention for the fabrication of optoelectronics, microwave devices, and integrated circuits used in modern high-speed optical communication system [1–5]. Metal–semiconductor (MS) contact is one of the most widely used rectifying contacts in the electronics industry [2–8]. The current–voltage (*I–V*) characteristics of the MS contacts usually deviate from the ideal thermionic emission (TE) current model [6–18]. Therefore, analysis of the *I–V* characteristics of the Schottky Barrier Diodes (SBDs) at room temperature only does not give detailed information about their conduction process or the nature of barrier formation at the MS interface. The temperature dependence of the *I–V* characteristics allows us to understand different aspects of conduction mechanisms [18–40]. Analysis of the *I–V* characteristics of SBDs based on TE theory usually reveals an abnormal decrease in the barrier height (BH), Φ_b and an increase in the ideality factor *n* with temperature decrease [24–39]. The decrease in the BH at low temperatures leads to nonlinearity in the activation energy $\ln(I_0/T^2)$ vs. $1/T$ plot.

The nature and origin of the decrease in the BH and increase in ideality factor with a decrease in temperature and all of the electrical anomalies in the SBDs may be attributed to the presence of Schottky barrier height (SBH) inhomogeneity [25–35]. An idea has been developed, that non-ideal behavior in the SBDs could be quantitatively explained by assuming specific distribution of nanometer-scale interfacial patches (small regions) with lower BH than the junction's main BH. In such cases, the current

across the MS contact may be greatly influenced by the presence of the SBH inhomogeneity [33–40]. Tung and coworkers [37, 38] have modeled imperfect Schottky contacts by assuming lateral variations of the BH. They [37, 38] found larger ideality factors and smaller effective BHs when they increased the inhomogeneity of barriers. Apart from the roughness of the interface due to thickness modulations of the metal as well as atomic steps, dislocations, and grain boundaries in the metal, these potential fluctuations may also originate from a local effective barrier lowering due to field emission at metallic diffusion spikes with narrow radii of curvature [27, 37, 38].

Consequently, two different approaches are adopted by researchers to describe the inhomogeneities [25–38]. One approach assumes a continuous distribution of the potential and the total current across a Schottky diode is simply calculated by integrating the current determined by the TE model with an individual BH and weighed by using the Gaussian distribution function [31–33]. This approach [31–33] does not address the lateral length scale of the inhomogeneity, the bias dependence of the SBH, namely, potential pinch-off, as stated in Refs. [37, 38]. The other approach [37, 38] assumes that small patches of low SBH are embedded in the uniform SBH area. In the present study, the *I–V* and *C–V* characteristics of Ag Schottky contacts on *n*-InP substrate were measured over the temperature range of 20–320 K by steps of 10 K. The temperature-dependent barrier characteristics of the diodes have been interpreted on the basis of a TE mechanism with Gaussian spatial distribution of BHs around a mean value due to barrier height inhomogeneities prevailing at the MS interface [31–33].

2 Experimental procedure

The Schottky barrier diodes were prepared using *n*-type InP (100) wafer. The carrier concentration values of 1.22×10^{15} and $1.32 \times 10^{15}\ \mathrm{cm}^{-3}$ for the *n*-type InP wafer were found from the experimental *C–V* data at 20 and 320 K, respectively. The wafer was degreased consecutively in trichloroethylene, acetone, and methanol for 5 min. The degreased wafer was etched with H_2SO_4:H_2O_2:H_2O (5:1:1) for 1 min to remove the surface damages and undesirable impurities. The back side ohmic contact was made by evaporating In and annealing at 320 °C under N_2 atmosphere for 3 min. The Schottky contacts with 1 mm diameter were formed on the front face of sample using a shadow mask. All evaporation processes were carried out in a vacuum coating unit at about 10^{-5} mbar. The *I–V* and *C–V* characteristics of the devices were measured in the temperature range of 20–320 K using a temperature controlled ARS Closed Cycle 4 K He cryostat, Temperature stability for each run was better than 0.1 K. Keithley 6514 electrometer and 2400 sourcemeter used for *I–V* measurements and Keithley 2400 sourcemeter and Boonton 72B capacitance meter used for *C–V* measurements.

3 Results and discussion

3.1 Temperature dependence of the forward bias *I–V* characteristics

We analyze the experimental *I–V* characteristics by the forward bias TE theory given as follows [2]

$$I = I_o \exp\left(\frac{q(V - IR_s)}{nkT}\right)\left[1 - \exp\left(-\frac{q(V - IR_s)}{kT}\right)\right], \quad (1)$$

where I_o is the saturation current derived from the straight line intercept of ln*I* at $V = 0$ and is given by

$$I_o = AA^*\ T^2 \exp\left(-\frac{q\Phi_{eff}}{kT}\right) \quad (2)$$

where q is the electron charge, V is the forward-bias voltage, R_s is the series resistance of the neutral region of the semiconductor bulk (between the depletion region and ohmic contact), IR_s is the voltage drop across the series resistance, A is the effective diode area, k is the Boltzman constant, T is the absolute temperature, A^* is the effective Richardson constant of $9.8\ \mathrm{Acm}^{-2}\ \mathrm{K}^{-2}$ for *n*-type InP [4], Φ_{eff} is the experimental zero bias BH (apparent barrier height) and n is the ideality factor. From Eq. 1, ideality factor n can be written as

$$n = \frac{q}{kT}\left(\frac{dV}{d\ \ln I}\right) \quad (3)$$

The semilog-forward and reverse bias *I–V* characteristics of the Au/*n*-InP SBDs are shown in the temperature range of 30–320 K by the steps of 10 K in Fig. 1. The forward bias *I–V* characteristics from 30 K to 200 K show a double slope structure whose reason will be discussed later. The saturation of the current at high biases in the forward bias is due to the series resistance of the neutral region of the device. The current at low temperatures consists of two regions indicating two parallel phases of Schottky barrier with different BHs [27, 41, 42]. The experimental values of Φ_{eff} (apparent barrier height) and n have been determined from intercepts and slopes of the forward-bias ln*I* vs. *V* plot at each temperature using the TE theory, respectively. The experimental forward bias *I–V* data in the temperature range of 200–320 K were fitted quite well over the whole bias by TE model (Eq. 1) taking Φ_{eff}, n and the series resistance R_s as adjustable parameters. However, the low temperature *I–V* characteristics show a double slope structure and cannot be fitted by Eq. 1 at the whole bias region, as seen in Fig. 1. That is, Φ_{eff} and n have been evaluated from the upper part with higher BH of the

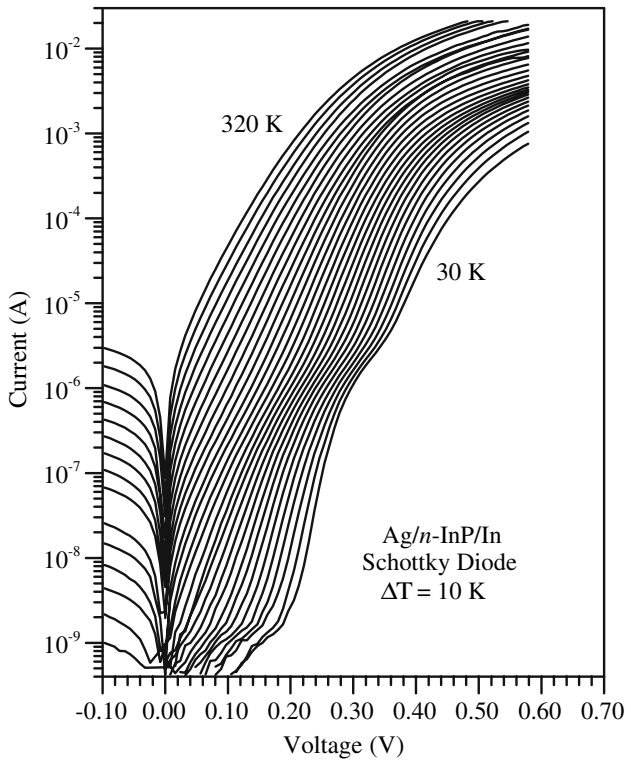


Fig. 1 Experimental reverse and forward bias current–voltage characteristics of an Ag/*n*-InP/In Schottky contact at various temperatures

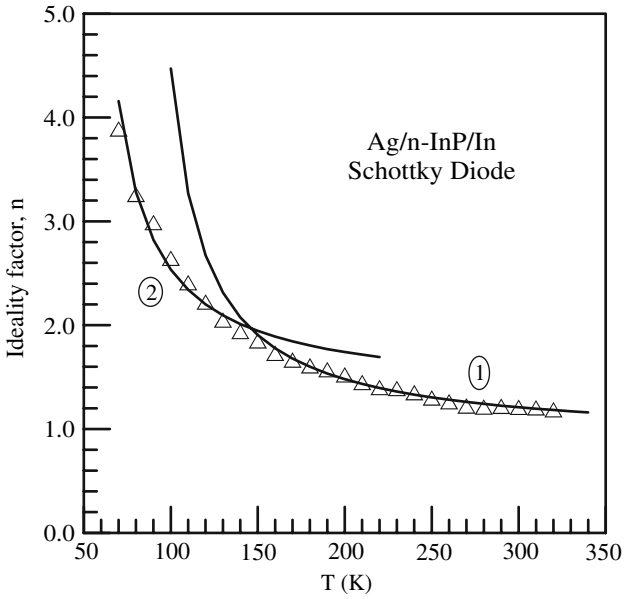


Fig. 2 Temperature dependence of the ideality factor (the open triangles) for Ag/*n*-InP/In Schottky diode. The continuous curves show estimated values of ideality factor using Eq. 9 for two Gaussian distributions of BHs with $\rho_2 = -0.128$, $\rho_3 = -0.016$ V in 150–320 K (the curve 1) and $\rho_2 = 0.246$, $\rho_3 = -0.006$ V in 80–140 K (the curve 2)

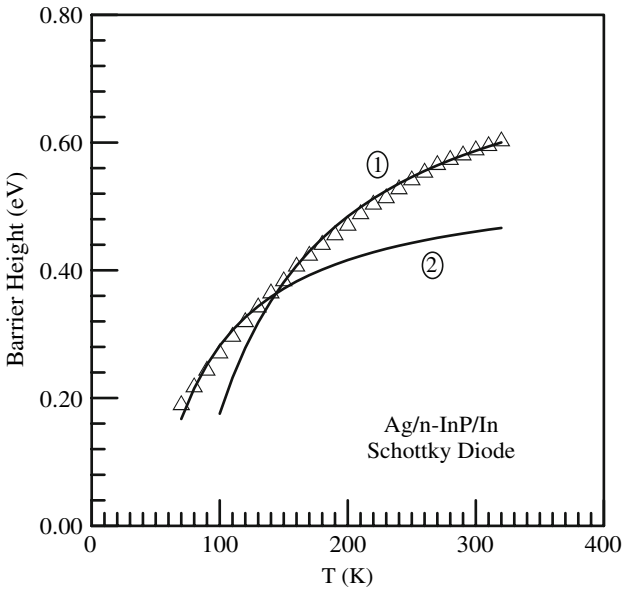


Fig. 3 Temperature dependence of and barrier height (the open triangles) for Ag/*n*-InP/In Schottky diode. The continuous curve related to the filled circles represents estimated values of Φ_{ap} using Eq. 8 for two Gaussian distributions of barrier heights with $\overline{\Phi}_{bo} = 0.79$ eV and $\sigma_s = 104$ mV in 150–320 K (the curve 1) and $\overline{\Phi}_{bo} = 0.55$ eV and $\sigma_s = 68$ mV in 70–150 K (the curve 2)

temperature-dependent forward bias *I–V* characteristics from 30 K to 200 K. For example, the experimental values of Φ_{eff} and n for the device were calculated as 0.61 eV and 1.18 at 320 K, 0.48 eV and 1.52 at 200 K, and 0.20 eV and 3.89 at 70 K, respectively. n and Φ_{eff} plots as a function of temperature are presented in Figs. 2 and 3, respectively. As can be seen, both parameters exhibit strong temperature dependence. That is, the apparent barrier height (BH) decreased and n increased with a decrease in temperature.

The values of n of 1.21 and 1.18 at 300 and 320 K, respectively, for this Ag/*n*-InP/In SBD indicate that the device obey a metal-interfacial layer-semiconductor (MIS) configuration rather than ideal Schottky diode. If the semiconductor surfaces are prepared by the usual polishing and chemical etching, and the evaporation of metal is carried out in a conventional vacuum system having a pressure of around 10^{-5} torr, their surfaces are inevitably covered with an undesirable native oxide film [1–6, 43]. Metal–semiconductor contacts formed under these conditions are not intimate contact because an interfacial layer of atomic dimensions inevitably separates them. Song et al. [31] have also suggested that the barrier inhomogeneities can occur as a result of inhomogeneities in the interfacial oxide layer composition, non-uniformity of the interfacial charges and interfacial oxide layer thickness. In such cases, the current across the MS contact may be greatly influenced by the presence of the SBH inhomogeneity [28–40]. Furthermore, some authors have mentioned that the ideality factor and the *I–V* BH (the saturation current) and

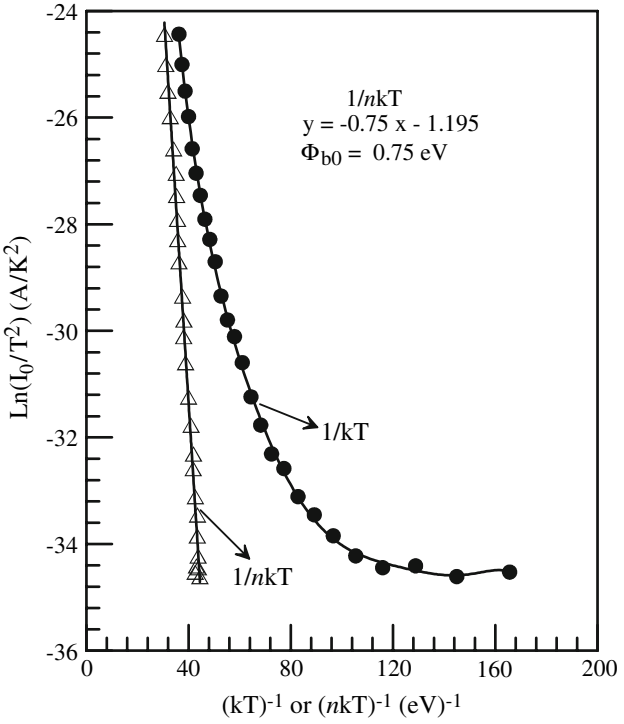


Fig. 4 Richardson plots of the $\ln(I_0/T^2)$ vs. $1/T$ (the filled circles) and $\ln(I_0/T^2)$ vs. $1/nT$ for the (the open triangles) for Ag/*n*-InP/In Schottky diode

all functions derived from them can also be explained and connected with the lateral distribution of BH due to local enhancement of electric field which can also yield a local reduction of the BH [27, 37, 42, 44].

The slope of the activation energy $\ln(I_0/T^2)$ vs. $1/kT$ plot allows the determination of the effective SBH according to Eq. 2. This plot is indicated by the closed circles in Fig. 4. Bowing of the experimental $\ln(I_0/T^2)$ vs. $1/T$ plot at low temperatures in Fig. 4 demonstrates that the fit of the experimental data is impossible for the determination of the effective SBH. Bowing of the experimental $\ln(I_0/T^2)$ vs. $1/T$ curve is caused by the temperature dependence of the BH and ideality factor. As will be discussed below, the deviation in the Richardson plots may be due to the presence of the spatially inhomogeneous BHs and potential fluctuations at the interface that consist of low and high barrier areas (located as patches in MS interface) [27, 35–39], that is, the current through the diode will flow preferentially through the lower barriers in the potential distribution [27, 36–40]. This lateral potential distribution of BH can be due to local enhancement of electric field which can also yield a local reduction of the BH [27, 36–40]. Likewise, the activation energy $\ln(I_0/T^2)$ vs. $1/nkT$ plot (open triangles) with the ideality factors was drawn, and this plot yielded a straight line with an activation energy value of 0.75 eV.

If the current transport is controlled by the thermionic field emission (TFE) theory, the relationship between the current and voltage can be expressed by [2, 3, 27]

$$I = I_0 \exp\left(\frac{qV}{E_0}\right) \tag{4}$$

with

$$n_{tun} = \frac{E_{00}}{kT}\coth\left(\frac{E_{00}}{kT}\right) = \frac{E_0}{kT} \tag{5}$$

where E_{00} is the characteristic tunneling energy that is related to the tunnel effect transmission probability:

$$E_{00} = \frac{h}{4\pi}\left(\frac{N_a}{m^*\varepsilon_s}\right)^{1/2}, \tag{6}$$

where $h = 6.626 \times 10^{-34}$ J.s, in the case of our *n*-type InP with $1.315 \times 10^{15}\,\mathrm{cm}^{-3}$, $m^* = 0.077m_o$ and $\varepsilon_s = 12.4\varepsilon_o$, and E_{00} was found to be about 0.69 meV. When considering the bias coefficient of the BH, $\beta = \partial\Phi_b/\partial V$, Eq. 5 can be written as [27, 44].

$$n_{tun} = \frac{E_0}{kT(1-\beta)} \tag{7}$$

Figure 5 represents the theoretical temperature dependence of ideality factor for the case when the current through Schottky junction is dominated by the TFE. The solid lines in Fig. 5 was obtained by fitting Eq. 7 to the experimental temperature dependence values of ideality factor presented for different values of the characteristic energy E_{00}, without considering the bias coefficient of the BH, $\beta = 0$. The open squares in the figure show the temperature dependence values of ideality factor obtained from the experimental current–voltage characteristics in Fig. 1. As can be seen from the figure, the experimental temperature dependence of ideality factor is in agreement with the curve (e) with $E_{00} = 23$ meV over the whole temperature range. This value of the characteristic energy value E_{00} is much higher than the theoretical value of 0.69 meV. This value seems unrealistically high for two reasons: first of all the theoretical value is 33 times smaller and secondly a study of Ag/*n*-InP Schottky diodes [42] gives an E_{00} of only 12 meV (roughly 1.2 times larger than the theoretical value) even though the net doping density is with about $2 \times 10^{17}\,\mathrm{cm}^{-3}$ 100 times larger than in the sample investigated in the present study. The net doping density of the InP sample is *only* $1.3 \times 10^{15}\,\mathrm{cm}^{-3}$, which means that tunnelling should not be highly relevant due to the width of the space charge region. Therefore, to analyze the temperature dependence of the BH and the ideality factor, let us apply the model of inhomogeneous BHs [31–34, 45].

The commonly observed deviation from classical TE theory, as will be discussed below, can be explained by a

recent model based on the assumption of a spatial fluctuation of the BH at interface [6–8, 19–35]. The continuous curves in Figs. 2, 3 and 6 and the linearity of the apparent BH and ideality factor versus $1/T$ curves in Fig. 6 show that the temperature dependence experimental data of the Ag/*n*-InP Schottky contact are in agreement with the recent model [31–34] which is the related to TE over a Gaussian BH distribution. The barrier height has a Gaussian distribution with the mean BH $\overline{\Phi}_b$ [8, 10, 15–17]. The Gaussian distribution of the BH yields the following expression for the BH: [31–33]:

$$\Phi_{ap} = \overline{\Phi}_b - \frac{q\sigma_s^2}{2kT}, \tag{8}$$

where Φ_{ap} is the apparent BH measured experimentally and σ_s is the standard deviation of the BH distribution. The temperature dependence of σ_s is usually small and can be neglected. The standard deviation is a measure of the barrier homogeneity. The above expression for the apparent BH construction was used already by Song et al. [31] and also by Werner and Güttler [32]. The observed variation of ideality factor with temperature in the model is given by [32]

$$\left(\frac{1}{n_{ap}} - 1\right) = -\rho_2 + \frac{q\rho_3}{2kT}, \tag{9}$$

where n_{ap} is apparent ideality factor and ρ_2 and ρ_3 quantify the voltage deformation of the BH distribution.

The experimental Φ_{ap} vs. $1/T$ and n_{ap} vs. $1/T$ plots (Fig. 6) drawn by means of the data obtained from Fig. 1 respond to two lines instead of a single straight line with transition occurring at 150 K. The linearity of the apparent BH or ideality factor versus $1/T$ curves in Fig. 6, and the continuous curves in Figs. 2 and 3 show that the temperature-dependent experimental data of the Ag/*n*-InP/In Schottky contact are in agreement with the recent model which is the related to thermionic emission over a Gaussian BH distribution [12–17]. Thus, the plot of Φ_{ap} vs. $1/T$ (Fig. 6) should be a straight line with the intercept at the ordinate determining the zero bias mean BH $\overline{\Phi}_{bo}$ and a slope giving the zero bias standard deviation σ_s. The above observations indicate the presence of two Gaussian distributions of BHs in the contact area. The intercept and slope of the straight line given two sets of values of $\overline{\Phi}_{bo}$ and σ_s as 0.79 eV and 105 mV in the temperature range of 150–320 K (the distribution 1), and as 0.55 eV and 68 mV in the temperature range of 70–150 K (the distribution 2). Furthermore, the Φ_{ap} values estimated from Eq. 8 over the entire temperature range of 70–320 K using the two $\overline{\Phi}_{bo}$ and σ_s are shown by the continuous curves 1 and 2 in Fig. 3. That is, the continuous solid lines related to the open triangles in Fig. 3 represent the data estimated using Eq. 8.

The existence of a double Gaussian in Schottky diodes was already experimentally proven by BEEM [46, 47]. These changes were also ascribed to the chemical treatment of the semiconductor surface [48–50]. Likewise, as indicated also by Chand and Kumar [51], the existence of a double Gaussian in the metal/semiconductor contacts can be attributed to the nature of the inhomogeneities themselves in the two cases. This may involve variation in the

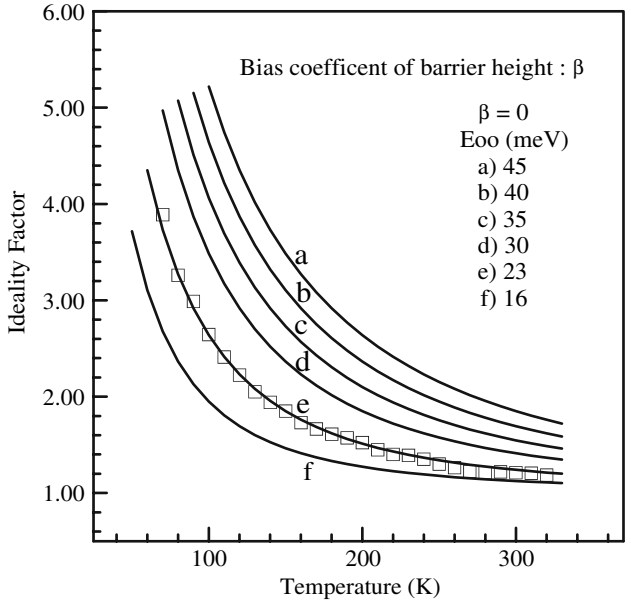


Fig. 5 Theoretical temperature dependence of ideality factor according to Eq. 7, the bias coefficient of barrier height, $\beta = 0$. The open squares show the experimental temperature dependence values of ideality factor obtained from the current–voltage characteristics given in Fig. 1

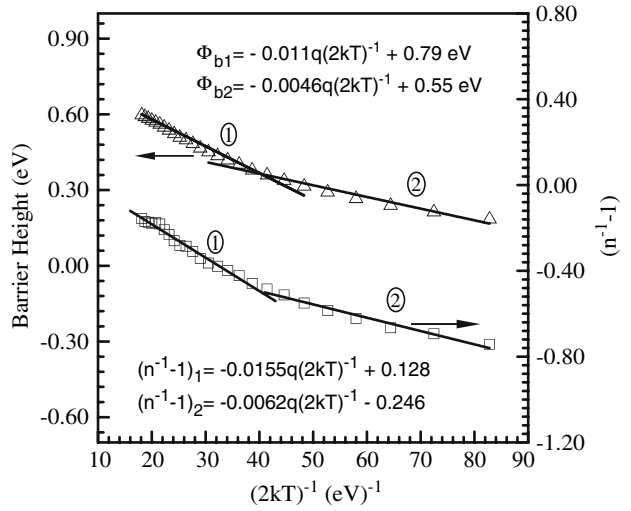


Fig. 6 Zero-bias apparent barrier height (the open triangles) and ideality factor (open squares) versus $1/(2kT)$ curves of the Ag/*n*-InP/In Schottky contact according to two Gaussian distributions of BHs. The data show linear variation in the two temperature ranges with a transition around 150 K

interface composition/phase, interface quality, electrical charges and non stoichiometry, etc. They are important enough to electrically influence the *I–V* characteristics of the Schottky diodes, at particularly low temperatures. Thus, *I–V* measurements at very low temperatures are capable of revealing the nature of barrier inhomogeneities present in the contact area. Furthermore, the temperature range covered by each straight line suggests the regime where the corresponding distribution is effective [51].

Moreover, as can be clearly seen from Fig. 6, the plot of n_{ap} vs. $1/T$ should also possess different characteristics in the two temperature ranges because the diode contains two BH distributions. The values of ρ_2 obtained from the intercepts of the experimental n_{ap} vs. $1/T$ plot are -0.128 in 150–320 K range (the distribution 1) and 0.246 in 70–150 K range (the distribution 2), whereas the values of ρ_3 from the slopes are -0.016 V in 150–320 K range and -0.006 V in 70–150 K range. The linear behavior of this plot demonstrates that the ideality factor indeed expresses the voltage deformation of the Gaussian distribution of the Schottky BH. The continuous solid lines in Fig. 2 represent data estimated with the above values of ρ_2 and ρ_3 using Eq. 9. As can be seen, the computed values exactly coincide with the experimental results in the respective temperature ranges for two different distributions. As can be seen from the n_{ap} vs. $1/T$ plot, ρ_3 value or the slope of the distribution 1 is larger than that of the distribution 2, therefore we may point out that the distribution 1 has wider and relatively higher BH. This is actually clear from the determined values of the mean BH and the standard deviation of distribution 1 and 2 which are given above. In additional to the explanations above, the regions with two different mean BHs exist for all temperatures investigated by us. The point is now that these two regions have different area ratio. From the data it seems clearly that the total area of regions with the lower mean BH (distribution 2) must be lower than that of the regions with higher mean BH (distribution 1). Therefore, we have found that the region with higher barrier height is dominant for higher temperatures (which would be impossible if the area ratio of regions with different barrier height was 1, in that case, the region with lower BH would dominate current transport).

The conventional activation energy $\ln(I_o/T^2)$ vs. $1/T$ plot has showed nonlinearity at low temperatures. To explain these discrepancies, according to the Gaussian distribution of the BH, we can be rewritten as

$$\ln\left(\frac{I_0}{T^2}\right) - \left(\frac{q^2\sigma_s^2}{2k^2T^2}\right) = \ln\left(AA^*\right) - \frac{q\overline{\Phi}_{bo}}{kT}, \qquad (10)$$

and a modified activation energy plot from this expression is obtained. Using the experimental I_0 data, a modified $\ln(I_0/T^2) - q^2\sigma_s^2/2k^2T^2$ vs. $1/T$ plot can be obtained according to Eq. 10 and should give a straight line with slope directly yielding the mean $\overline{\Phi}_{bo}$ and the intercept $(= \ln AA^*)$ at the ordinate determining A^* for a given diode area A. The $\ln(I_0/T^2) - q^2\sigma_s^2/2k^2T^2$ values were calculated for both two values of σ obtained for the temperature ranges of 70–150 K and 150–320 K. Thus, the open triangles and open squares in Fig. 7 have given the modified $\ln(I_0/T^2) - q^2\sigma_s^2/2k^2T^2$ vs. $1/T$ plots for both two values of σ. The best linear fitting to these modified experimental data are depicted by solid lines in Fig. 7 which represent the true activation energy plots in respective temperature ranges. The calculations yielded zero bias mean BH$\overline{\Phi}_{bo}$ of 0.55 eV (in the range of 70–150 K) and 0.79 eV (in the range of 150–320 K). These values match exactly with the mean BHs obtained from the Φ_{ap} vs. $1/T$ plot in Fig. 6. The intercepts at the ordinate give the Richardson constant A^* as 8.18 A/cm^{2}K^2 (in 70–150 K range) and 7.96 A/cm^{2}K^2 (in 150–320 K range) without using the temperature coefficient of the BHs. The obtained Richardson constant values are in close agreement with the known value of 9.8 A/cm^{2}K^2 for *n*-type InP.

Figure 8 shows the reverse bias C^{-2}–V characteristics in the temperature range of 20–320 K by the steps of 20 K. Figure 9 shows Φ_{C-V} (indicated by open triangles) values

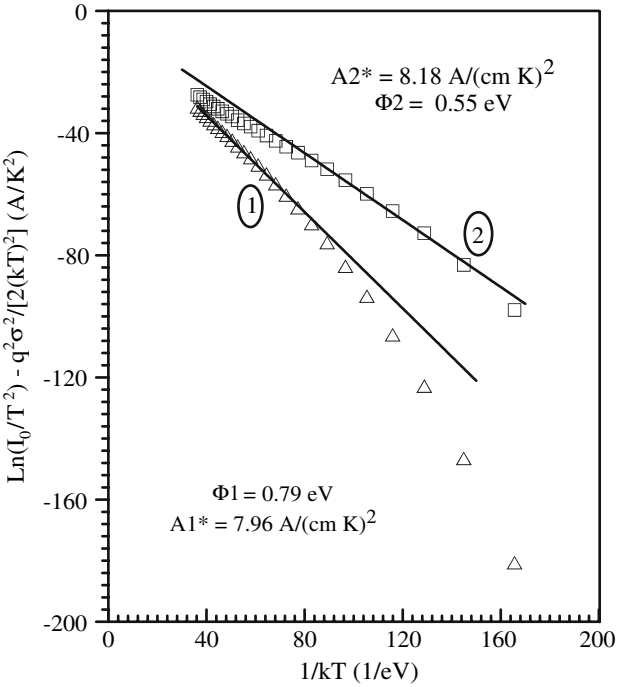


Fig. 7 Richardson plot of the $\ln(I_0/T^2)$ vs. $1/T$ plot (the open triangles) and modified Richardson $\ln(I_0/T^2) - q^2\sigma_s^2/2k^2T^2$ vs. $1/T$ plot for the Ag/*n*-InP/In Schottky diode according to two Gaussian distributions of barrier heights. The open squares represent the plot calculated for $\sigma_s = 68$ mV and the open triangles represent the plot calculated for $\sigma_s = 104$ mV. The straight lines 1 and 2 indicate the best fitting of the data in temperature ranges of 150–320 K and 70–150 K, respectively

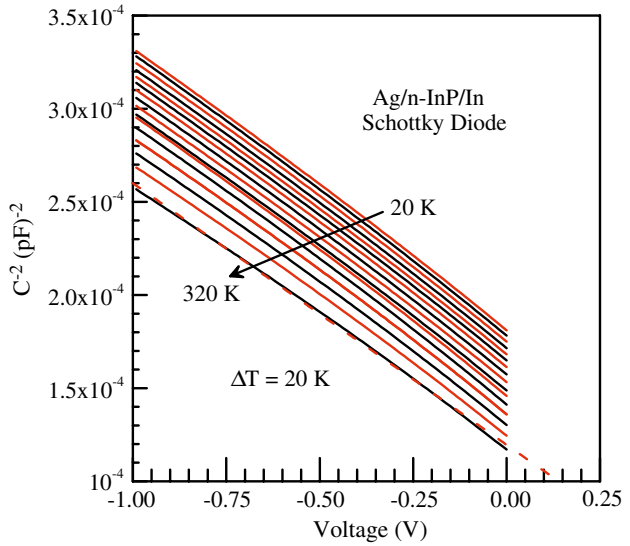


Fig. 8 Experimental reverse bias C^{-2}–V characteristics of a typical Ag/n-InP/In Schottky diode at various temperatures

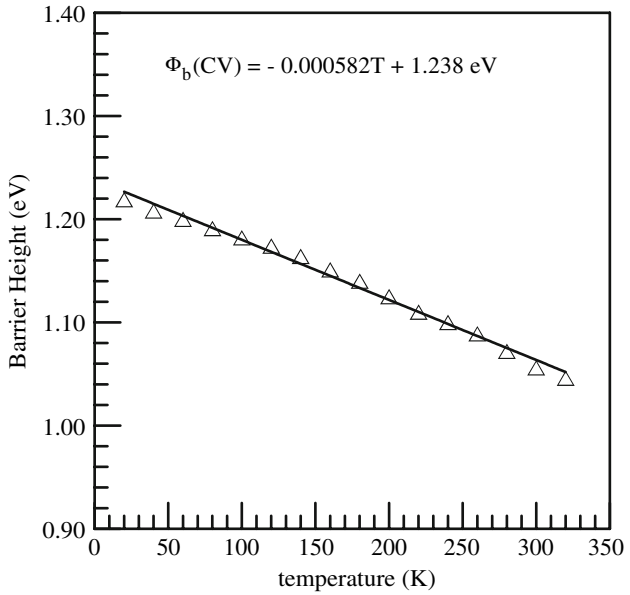


Fig. 9 Temperature dependence of the C–V barrier height from experimental reverse bias C^{-2}–V characteristics (Fig. 8) for a typical Ag/n-InP/In Schottky diode

obtained from the reverse bias C^{-2}–V characteristics (Fig. 8) depending on the temperature. The experimental Φ_{C-V} vs. T plot yields $\Phi_{C-V}\ (T=0) = 1.24$ eV and $\alpha = -0.582$ meV/K, where α is the temperature coefficient of the BH. Furthermore, the experimental values of Φ_{C-V} for the device were calculated as 1.05 eV at 320 K, 1.13 eV at 200 K, and 1.22 eV and at 20 K, respectively. Moreover, the temperature dependence of the experimental carrier concentration was calculated from the reverse bias C^{-2}–V characteristics in Fig. 8 and this plot is given in Fig. 10. For example,

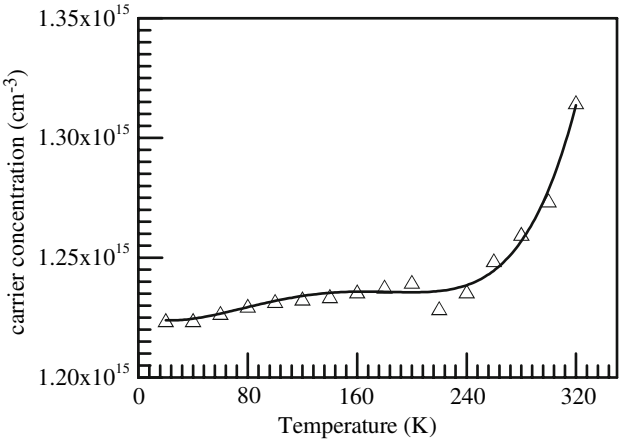


Fig. 10 Temperature dependence of the carrier concentration from experimental reverse bias C^{-2}–V characteristics (Fig. 8) for typical Ag/n-InP/In Schottky diode

these values were 1.224×10^{15} and 1.315×10^{15} cm^{-3} for the n-type InP wafer at 20 and 320 K. As can be seen from Fig. 10, the carrier concentration of the n-InP slightly decreased with a decrease in temperature in the range of 20–200 K while it more decreased with decreasing temperature in the range of 200–320 K. The solid lines are used for fits to the experimental data.

The difference between the BH values from the C^{-2}–V and I–V characteristics is larger than the image force lowering value of 0.014 eV for this device. The image force lowering value for the BH was determined by using Eq. 1.26a in Ref. [2]. Although this discrepancy could be explained by the existence of an interfacial layer or of trap states in the semiconductor [32, 37, 38], the existence of Schottky BH inhomogeneity offers another explanation [32, 37, 38]. The capacitance C is insensitive to potential fluctuations on a length scale of less than the space-charge width and the C–V method averages over the whole area. The dc current I across the interface depends exponentially on Φ_b and thus sensitively the detailed barrier distribution at the interface. Any spatial variation in the barriers causes the current I to flow preferentially through the barrier minima. That is, the current in the I–V measurement is dominated by the current which flows through the region of low SBH. Since the low-SBH patch is pinched-off, the effective SBH of the patch is the potential at the saddle point [37, 38]. Consequently, for an inhomogeneous interface, the spatial variation of the band bending results in different BH for the current and capacitance, and the capacitances are expected to measure only the mean BH value [32, 37, 38]

In conclusion, the apparent BH, Φ_{bo}, from the current–voltage (I–V) characteristics of the Ag/n-InP/In Schottky contact decreases while the ideality factor n increases with

a decrease in temperature due to the barrier inhomogeneity or to local enhancement of electric field which can also yield a local reduction of the BH. The activation energy $\ln(I_0/T^2)$ vs. $1/nkT$ plot yielded a straight line with an effective BH value of 0.75 eV. The modified $\ln(I_0/T^2) - q^2\sigma_s^2/2k^2T^2$ vs. $1/T$ plots yielded zero bias mean BH$\overline{\Phi}_{bo}$ of 0.55 eV (in the range of 70–150 K) and 0.79 eV (in the range of 150–320 K). These values match exactly with the mean BHs obtained from the Φ_{ap} vs. $1/T$ plot. The modified activation energy plot from the barrier inhomogeneity model have given the Richardson constant A^* as 8.18 A/cm^{2}K^2 and 7.96 A/cm^{2}K^2. It has been seen that he obtained Richardson constant values are in close agreement with the known value of 9.8 A/cm^{2}K^2 for n-type InP.

Acknowledgments This work was supported by The Turkish Scientific and Technological Research Council of Turkey (TUBITAK) (Project No: 105T487) and Atatürk University (Project No: BAP 2006/51). The Authors wish to thank to TUBITAK and Atatürk University.

References

1. M. Oztas, M. Bedir, R. Kayalı, F. Aksoy, Mater. Sci. Eng. B **131**, 94 (2006)
2. E.H. Rhoderick, R.H. Williams, *Metal–Semiconductor Contacts* (Clarandon Press, Oxford University Press, 1988)
3. R.H. Williams, G.Y. Robinson, in *Physics and Chemistry of III–V Compound Semiconductor Interfaces*, ed. by C.W. Wilmsen (Plenum Press, New York 1985)
4. H. Cetin, E. Ayyildiz, Semicond. Sci.Technol. **20**, 625 (2005); Appl. Surf. Sci. **253**, 5961 (2007); H. Cetin, E. Ayyildiz, A. Turut, J. Vac. Sci. Technol. B **23**, 2436 (2005)
5. R.L. Van Meirhaeghe, W.H. Laflére, F. Cardon, J. Appl. Phys. **76**, 403 (1994)
6. M.E. Aydin, N. Yıldırım, A. Turut, J. Appl. Phys. **102**(4), 043701 (2007)
7. A. Sellai, M. Mamor, Appl. Phys. A **89**, 503 (2007); M. Mamor, A. Sellai, K. Bouziane, S.H. Al Harthi, M. Al Busaidi, F.S. Gard, J. Phys. D: Appl. Phys. **40**, 1351 (2007)
8. A.R. Arehart, B. Moran, J.S. Speck, U.K. Mishra, S.P. DenBaars, S.A. Ringel, J. Appl. Phys. **100**, 023709 (2006)
9. D.M. Kim, D.H. Kim, S.Y. Lee, Solid-State Electron. **51**, 865 (2007)
10. A.F. Qasrawi, Semicond. Sci. Technol. **21**, 794 (2006)
11. M.M. El-Nahass, H.M. Zeyada, K.F. Abd-El-Rahman, A.A.A. Darwish, Sol. Energy Mater. Sol. Cells **91**, 1120 (2007)
12. N. Rouag, L. Boussouar, S. Toumi, Z. Ouennoughi, M.A. Djouadi, Semicond. Sci. Technol. **22**(4), 369 (2007)
13. R. Pérez, N. Mestres, J. Montserrat, D. Tournier, P. Godignon, Phys. Stat. Sol. (a) **202**(4), 692 (2005)
14. M. Ozer, D.E. Yildiz, S. Altindal, M.M. Bulbul, Solid-State Electron. **51**(6), 941 (2007)
15. F. Roccaforte, F. La Via, V. Raineri, R. Pierobon, E. Zanoni, J. Appl. Phys. **93**(11), 9137 (2003)
16. C.F. Pirri, S. Ferrero, L. Scaltrito, D. Perrone, S. Guastella, M. Furno, G. Richieri, L. Merlin, Microelectron. Engineer. **83**, 86 (2006)
17. K.V. Vassilevski, I.P. Nikitina, N.G. Wright, A.B. Horsfall, A.G. O_Neill, C.M. Johnson, Microelectron. Eng. **83**, 150 (2006)
18. M. Pattabi, S. Krishnan, Ganesh, X. Mathew, Sol. Energy **81**(1), 111 (2007); M. Pattabi, S. Krishnan, G. Sanjeev, Sol Energ Mat Sol C **91**, 1521 (2007)
19. I. Dokme, S. Altindal, M.M. Bulbul, Appl. Surf. Sci. **252**(22), 7749 (2006); I. Dokme, S. Altindal, Semicond. Sci. Technol. **21**(8), 1053 (2006)
20. F. Yakuphanoglu, Physica B **389**(2), 306 (2007)
21. S. Kumar, Y.S. Katharria, S. Kumar, D. Kanjilal, J. Appl. Phys. **100**, 113723 (2006)
22. F. Brovelli, B.L. Rivas, J.C. Bernede, J. Chilean Chem. Soc. **52**(1), 1065 (2007)
23. N.L. Dimitruk, O.Yu. Borkovskaya, I.N. Dimitruk, S.V. Mamykin, Zs.J. Horvath, I.B. Mamontova, Appl. Surf. Sci. **190**, 455 (2002)
24. S.W. Kim, K.M. Lee, J.H. Lee, K.S. Seo, IEEE Electron Device Lett. **26**(11), 787 (2005)
25. H. von Wenckstern, G. Biehne, R.A. Rahman, H. Hochmuth, M. Lorenz, M. Grundmann, Appl. Phys. Lett. **88**(9), 092102 (2006)
26. J. Osvald, Z.J. Horvath, Appl. Surf. Sci. **234**(1–4), 349–354 (2004)
27. Zs.J. Horváth, Solid-State Electron. **39**, 176 (1996); E. Ayyildiz, H. Cetin, Zs.J. Horvath, Appl. Surface Sci. **252**, 1153 (2005)
28. F.E. Jones, C.D Hafer, B.P. Wood, R.G. Danner, M.C. Lonergan, J. Appl. Phys. **90**, 1001 (2001)
29. H.J. Im, Y. Ding, J.P. Pelz, W.J. Choyke, Phys. Rev. B, **64**(7), 075310 (2001)
30. R.C. Rossi, N.S. Lewis, J. Phys. Chem. B **105**(17), 12303 (2001)
31. Y.P. Song, R.L.Van Meirhaeghe, W.H. Laflére, F. Cardon, Solid-State Electron. **29**, 633 (1986)
32. J.H. Werner, H.H. Güttler, J. Appl. Phys. **69**, 1522 (1991)
33. S. Chand, J. Kumar, J. Appl. Phys. **82**, 5005 (1997); S. Chand, S. Bala, Appl. Surf. Sci. **252**, 358 (2005); S. Chand, J. Kumar, Appl. Phys. A **65**, 497 (1997)
34. S. Zhu, R.L. Van Meirhaeghe, S. Forment, G. Ru, B. Li, Solid-State Elecron. **48**, 29 (2004)
35. J. Osvald, J. Appl. Phys. **85**(3), 1935 (1999); E. Dobrocka, J. Osvald, Appl. Phys. Lett. **65**, 575 (1994); J. Osvald, Solid-State Electron. **50**, 228 (2006)
36. H. Dogan, N. Yıldırım, A. Turut, M. Biber, E. Ayyıldız, C. Nuhoglu, Semicond. Sci.Technol. **21**, 822 (2006)
37. R.T. Tung, Phys. Rev. B. **45**, 13509 (1992)
38. J.P. Sullivan, R.T. Tung, M.R. Pinto, W.R. Graham, J. Appl. Phys. **70**, 7403 (1991)
39. S. Huang, B. Shen, M.J. Wang, F.J. Xu, Y. Wang, H.Y. Yang, F. Lin, L. Lu, Z.P. Chen, Z.X. Qin, Z.J. Yang, G.Y. Zhang, Appl. Phys. Lett. **91**, 072109 (2007)
40. A. Gümüş, A. Türüt, N. Yalçın, J. Appl. Phys. **91**, 245 (2002)
41. N. Newman, M. van Schilfgaarde, T. Kendelewicz, D.M. Williams, W.E. Spicer, Phys. Rev. **B33**, 1146 (1986)
42. Zs.J. Horvath, J. Appl. Phys. **64**, 6780 (1988)
43. T. Teraji, S. Hara, Phys. Rev. B **70**, 035312 (2004)
44. Zs.J. Horvath, V. Rakovics, B. Szentpali, S. Puspoki, K. Zdansky, Vacuum **71**, 113 (2003)
45. S. Karatas, S. Altındal, A. Türüt, A. Özmen, Appl. Surf. Sci. **217**, 250 (2003)
46. G.M. Vanalme, L. Goubert, R.L. Van Meirhaeghe, F. Cardon, P. van Daele, Semicond. Sci. Technol. **14**, 871 (1999)
47. G.M. Vanalme, R.L. van Meirhaeghe, F. Cardon, P. van Daele, Semicond. Sci.Technol. **12**, 907 (1997)
48. A.R.V. Roberts, D.A. Evans, Appl. Phys. Lett. **86**, 072105 (2005)
49. T.U. Kampen, S. Park, D.R.T. Zahn, Appl. Surf. Sci. **190**, 461 (2002)
50. T. Kampen, A. Schuller, D.R.T Zahn, B. Biel, J. Ortega, R. Perez, F. Flores, Appl. Surf. Sci. **234**(1–4), 341 (2004)
51. S. Chand, J. Kumar, Semicond. Sci.Technol. **11**, 1203 (1996)